



The Use Of Electrochemical Impedance Spectroscopy (EIS) And Vibrating Sample Magnetometer (VSM) For Measuring The Corrosion Rate Of Polymer-Coated Ferromagnetic Metals.

To cite this article: (2001) The Use Of Electrochemical Impedance Spectroscopy (EIS) And Vibrating Sample Magnetometer (VSM) For Measuring The Corrosion Rate Of Polymer-Coated Ferromagnetic Metals. , Materials Technology, 16:2, 90-97, DOI: [10.1080/10667857.2001.11752917](https://doi.org/10.1080/10667857.2001.11752917)

To link to this article: <https://doi.org/10.1080/10667857.2001.11752917>



Published online: 25 Aug 2016.



Submit your article to this journal [↗](#)



Article views: 15



Citing articles: 2 View citing articles [↗](#)

The Use Of Electrochemical Impedance Spectroscopy (EIS) And Vibrating Sample Magnetometer (VSM) For Measuring The Corrosion Rate Of Polymer-Coated Ferromagnetic Metals.

Electrochemical impedance spectroscopy (EIS) has some significant drawbacks with regard to *in situ* measurements of the corrosion rate beneath a polymer coating. The vibrating sample magnetometer (VSM) can be used to measure the saturation magnetic moment (μ_s) of ferromagnetic materials, thus indicating their mass (volume). A novel approach is introduced in this work to monitor the corrosion of bare and acrylic-coated cobalt *in situ* and in real time by coupling EIS and VSM. This combination is found to be powerful when the corrosion products are not ferromagnetic. For the first time, the corrosion rate beneath a polymer coating is measured accurately *in situ*. Furthermore, it is suggested that the VSM can be used to enhance the interpretation of EIS data.

Introduction

Organic coatings are often used as physical barriers between substrates and corrosive environments, although they may also serve as reservoirs for inhibiting compounds. Nevertheless, such coatings are not impervious to aqueous solutions, which might ultimately lead to the insidious phenomenon of underfilm corrosion. The corrosion rate cannot be assessed in this case by direct weight loss measurements due to water absorption in the coating, trapping of corrosion products beneath the coating, and the non-uniform character of underfilm corrosion.

EIS has been widely used to study corrosion protection by organic coatings. Advantages of this technique over *dc* and conventional techniques include the absence of any significant perturbation to the system, its applicability to the assessment of low-conductivity media such as polymers, and the existence of a frequency component that may provide mechanistic information. EIS, however, has some significant drawbacks. At low frequencies, where underfilm corrosion reactions are probed, experimental difficulties and time constraints can complicate precise determination of the charge-transfer

resistance (R_{ct} , describing the electrochemical reaction under activation control) and the double-layer capacitance (C_{dl} , formed by the electrolyte phase beneath the coating); additionally, the Warburg impedance may have a masking effect, and inductive loops or new time constants are sometimes observed. Moreover, due to the long measurement time required, both the corrosion rate and corrosion potential can change during the experiment. There has also been no evidence that R_{ct} can be equated to the polarization resistance (R_p , the faradaic reaction resistance) and used in the Stern-Geary equation to calculate the underfilm corrosion rate. In-depth mechanistic and kinetic information on the corroding interface can easily be overlooked in EIS by modeling the system with an oversimplified equivalent circuit. Finally, although it is possible to determine by EIS when the interface becomes electrified, it is not, at present, possible to determine unambiguously the origin of the electrification.

Magnetic measurements may also be used to monitor corrosion. The saturation magnetic moment (μ_s) of a ferromagnetic material is a structure-insensitive material property; thus, it only changes with mass (volume) of the material. Since the signal from a ferromagnetic substrate is much larger than the signals of either a polymer coating or non-ferromagnetic corrosion products, decreases in μ_s can be measured and used to assess the mass loss due to corrosion]. In principal, the measurement of such decreases can be used to distinguish between delamination of coatings due to loss of adhesion or due to corrosion at the metal-polymer interface.

The VSM, invented by Foner of MIT, has been used since the late 1950's to investigate the magnetic properties of materials. Its operating principle involves the detection of a dipole field from a magnetic sample when it is vibrated perpendicularly to a uniform magnetizing field. Since changes of magnetic moment as small as 10^{-5} - 10^{-6} emu can be detected, this technique can monitor very low mass losses (as low as a few micrograms). In addition to being non-destructive and permitting convenient measurements using commercial electromagnets, this technique is highly accurate.

The objective of this work is twofold: to verify the applicability of the VSM for measuring the corrosion rate of bare and coated ferromagnetic materials, and to suggest a way of using it to enhance the interpretation of EIS data. Once a correlation between electrochemistry and mass loss is unequivocally established, there will no longer be any obstacle to the use of EIS for monitoring the corrosion rate of an organic-coated metal.

Experimental Details

Cobalt was chosen for this work since it is ferromagnetic

and corrodes to produce non-ferromagnetic oxides. For instance, cobaltous oxide (CoO) and cobalto-cobaltic oxide (Co₃O₄) are both known to be paramagnetic.

Sample size was an important consideration in this research. On the one hand, since small amounts of corrosion were expected (given the presence of a coating and short exposure times), the initial volume of the cobalt had to be sufficiently small to ensure significant change in saturation magnetic moment; *i.e.*, larger than the sensitivity of the VSM ($\pm 0.25\%$). In addition, the sample had to be placed within a reduced VSM pole gap (to achieve increased magnetic fields) and satisfy the magnetic dipole approximation. The need to achieve increased magnetic fields mainly results from the strong magnetic anisotropy of cobalt; there is only one easy axis of magnetization, which corresponds to the [0001] axis of hexagonal symmetry. Consequently, the experimental intrinsic magnetization curves depend on the relative orientation of the magnetic moments in the sample to the applied field. However, at sufficiently high applied fields, the saturation magnetic moment is the same for all different orientations.

Sample size, on the other hand, needed to be large enough to avoid ohmic errors during electrochemical tests due to sheet resistance phenomena, and to provide a sufficiently large exposed area for the electrochemical measurements to be meaningful.

To prepare the samples, silicon wafers were electron-beam deposited with a 3200 Å-thick pure cobalt layer at MIT's Microsystems Technology Laboratory. The thickness of the cobalt layer was measured by a Tencor-KLA P10 profilometer. The wafers were then sectioned into rectangular samples of approximately 0.7 cm by 2.3 cm. Selected samples were coated with a transparent acrylic varnish. The polymer coating was prepared by mixing 100 g Viacryl VSC 5754/60 resin with 36g Maprenal MF800, both from Vianova Resins. Acetone was added to the mixture to attain the proper viscosity. The samples were subsequently dipped in a bath of the varnish and allowed to air-dry for a short time prior to curing in an oven at 115°C for 30 min. The polymer was undercured on purpose to make it more permeable to moisture and ions by decreasing the degree of cross-linking. Attaching a shielded copper wire to the cobalt by means of tin soldering produced an electrical contact for the electrochemical measurements. A glass capillary was used to protect the copper wire from undergoing underfilm corrosion beneath its insulation sheath. The soldered edge of the sample and the end of the capillary were covered by a small amount of five-minute epoxy glue to prevent galvanic corrosion between cobalt, copper and tin, and to provide good mechanical bonding between the sample and the capillary. Finally, the back and the edges of the sample

were masked with gray paint (Ameron's Amercoat 90) to prevent localized corrosion phenomena.

VSM and EIS tests were performed *in situ* and in real time on the cobalt samples using a novel miniature cell design (Figure 1). This cell design satisfied the previous sample dimension requirements and used weakly diamagnetic and paramagnetic materials. A Pyrex tube of 11 mm inner diameter and 13 mm outer diameter was cut to a length of approximately 45 mm. One end of the tube was dipped in a five-minute epoxy gel. After the solid epoxy plug was established, three holes of adequate diameter were drilled to permit positioning of the inner components. The sample and a platinum electrode, the latter serving as a counter/auxiliary electrode in electrochemical measurements, were glued inside the tube, facing each other. The platinum electrode was prepared in advance by spark welding a high-purity platinum wire to a high-purity platinum foil. The bottom end of the tube and the two holes through which the sample and the counter electrode were inserted were subsequently sealed with epoxy. A glass rod was glued along the axis of the cell and a removable plastic plug was adjusted to seal the third hole during VSM runs.

The cell was filled with a 0.5 M NaCl (pH 7) solution, daily refreshed from a reservoir through which purified air was continuously bubbled. For EIS measurements, a modified three-electrode setup was used, in which a Ag/AgCl miniature reference electrode (EG&G model K0265) was immersed directly in the cell. The standard potential of the relevant half-cell reaction is +0.222 V *vs.* SHE (standard hydrogen electrode). The electrode was filled with a solution of 17%, 3 M NaCl in distilled water, saturated with AgCl. Under such conditions, the electrode potential is +0.194 V *vs.* SHE. A Schlumberger Solartron 1286 Electrochemical Interface and a Solartron 1250 Impedance / Gain-Phase Analyzer, connected to a PC by an IEEE/GPIB interface, were used. EISTEST, a software package developed at the H.H. Uhlig Corrosion Laboratory, was used to control the sweeps. The open circuit potential (OCP) was monitored for more than 20 minutes before each sweep. Frequency ranges of 10 kHz to 10 mHz and 65 kHz to 5 mHz were selected for the uncoated and polymer-coated samples, respectively. The amplitudes of the superimposed potential were 5 and 20 mV for the uncoated and coated samples, respectively. EIS data was analyzed with ZView, a software package developed by Scribner Associates.

Potentiodynamic measurements were carried out with a traditional three-electrode setup in order to estimate the Tafel slopes for bare cobalt. A 0.5 M NaCl solution and a saturated calomel electrode (SCE) were used. Before each measurement, the OCP was monitored for at least 10 min. Scans were

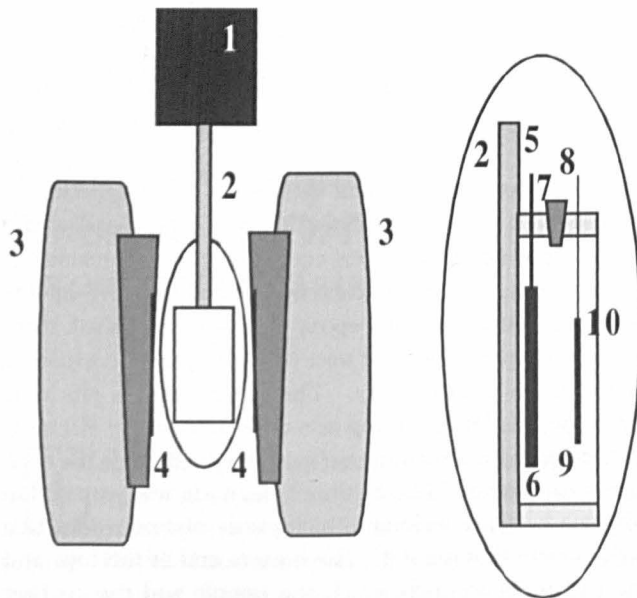


Figure 1: Schematic of the miniature cell (circled) as positioned in the VSM.

1 – vibration unit; 2 – glass rod (cell holder); 3 – magnet; 4 – magnet poles with pickup coils; 5 – shielded copper wire surrounded by glass capillary; 6 – sample; 7 – conical plastic plug (removable to allow electrolyte refreshment and/or introduction of a miniature reference electrode for EIS measurements); 8 – pure platinum wire; 9 – pure platinum foil (counter electrode in electrochemical measurements); 10 – Pyrex tube; 11 – five-minute epoxy plug.

subsequently generated from -250 mV relative to the OCP to $+700$ mV (with respect to the SCE), at a sweep rate of 1 mV/s, using Scribner Associates' DC Corrware software package.

Corrosion rates were obtained from electrochemical measurements, using the expression:

$$r = \frac{a \cdot i_{\text{corr}}}{nF} \quad (1)$$

where a is the atomic mass of the corroded metal (58.933 g/mol), n the number of electrons transferred in the reaction (2 equiv./mol), F is Faraday's constant ($96,487$ C/equiv.), and i_{corr} the corrosion current density. Substituting the Stern-Geary relation for i_{corr} , the following equation is obtained:

$$r = \frac{a}{nFAR_p} \cdot \frac{\beta_a |\beta_c|}{2.3(\beta_a + |\beta_c|)} \quad (2)$$

where A is the exposed surface area, R_p the polarization resistance, and β_a and β_c the anodic and cathodic Tafel slopes, respectively. The cumulative mass loss was subsequently obtained by integrating the normalized time-dependent

corrosion rate on time:

$$\Delta m = \int_{t_0}^{t_n} r A dt \quad (3)$$

Magnetic measurements were carried out at room temperature with a Model 880 VSM from Digital Measurement Systems, Inc. The instrumentation was controlled by a commercial software package written in Visual BASIC and capable of measuring all basic magnetic properties. Firstly, calibration was carried out using a standard high-purity nickel disc. The voltage gain of the VSM was automatically redefined to obtain a standardized value for the reference sample. Secondly, the reference electrode was removed from the miniature cell, and the cell was entirely filled with solution, sealed with a conical plug and tightly mounted onto a glass rod (cell holder). Thirdly, the sample was positioned at the saddle point of the magnetic field. Finally, the magnetic moment of each cell was recorded six times in the range $8,050$ - $10,000$ Oe. To collect the magnetic moment data, an averaging technique was employed, in which the average moment value was computed over thirty measurements every 50 Oe. Eventually, the saturation magnetic moment (μ_s) was calculated by averaging the values obtained from four of the six runs, ignoring the other two extreme values. Employing this procedure, very accurate values of μ_s were obtained; typically with $STDEV / \bar{\mu}_s < 0.25\%$, where $STDEV$ is the standard deviation and $\bar{\mu}_s$ the mean saturation magnetic moment.

The total magnetic moment of the system, $\mu(H)$, included contributions from the ferromagnetic cobalt and from all of the remaining paramagnetic and diamagnetic materials present in the cell. This can be expressed by:

$$\mu(H) = (1-\alpha) \times V_0 \times M(H) + (\sum \alpha_i V_0 \chi_i + V_p \chi_p + \sum V_j \chi_j) \cdot H \quad (4)$$

where $\alpha \equiv \sum \alpha_i$ is the volume fraction of cobalt that has been corroded/oxidized, α_i the volume fraction of cobalt that has turned into a corrosion/oxidation product i , V_0 the initial volume of ferromagnetic Co, $M(H)$ the magnetization of Co, H the applied magnetic field, χ_i the magnetic susceptibility of the i^{th} corrosion/oxidation product, V_p the volume of the polymer coating, χ_p the magnetic susceptibility of the polymer, V_j the volume of the material of the j^{th} constituent of the cell (other than cobalt, polymer coating, and corrosion/oxidation products), and χ_j its magnetic susceptibility.

When the applied field exceeds the saturating field of the ferromagnetic material, the magnetization is no longer

dependent on the applied field; *i.e.*, $M(H) \equiv M_s$, the saturation magnetization (the maximal magnetic moment density). Thus, the signal of the system becomes a straight line, and μ_s of cobalt can be separated readily from the contributions of the paramagnetic and diamagnetic materials by linear regression.

It should be noted that intrinsic magnetization curves were recorded for the different constituents of the cell. The Pyrex tube, made from a diamagnetic material, exhibited good linearity with a reasonably low slope of approximately -1.0×10^{-7} emu/Oe. The platinum electrode, made from a paramagnetic material, also revealed excellent linearity with a slope of approximately 5.0×10^{-7} emu/Oe. The electrolyte (0.5 M NaCl) exhibited exceptional linearity with a slope of the order of -2.0×10^{-7} emu/Oe. The remaining constituents of the cell (gray paint, epoxy, solder material, glass rod, glass capillary, copper wire, plastic conical plug, and silicon wafer) all exhibited negligible signals (lower than 10^{-5} emu) when tested individually. Due to compensations between the diamagnetic and the paramagnetic materials, the slope of the linear signal from the cell filled with electrolyte was approximately 2.0×10^{-7} emu/Oe. The signal from the cobalt sample ($\sim 3.5 \times 10^{-2}$ emu) was thus prominent within the range of 8,050-10,000 Oe.

Several other factors are noteworthy with regard to the magnetic measurements. First, the core of the cell was chosen to be a long hollow cylinder of semi-infinite geometry in order to minimize disruptions of the magnetic flux lines. Second, the core was glued to a glass rod to prevent any relative rotation between the cell and its holder. Third, to avoid effects of dynamic resonance due to extra vibrations under the VSM, the cell was entirely filled with electrolyte and sealed with a plug. Moreover, cobalt is an extremely stable ferromagnetic material, with a Curie temperature as high as 1115°C . In the vicinity of room temperature, where all measurements were carried out, the variation of M_s with temperature is infinitesimal. Another factor to be considered is the volume of the sample. The saturation magnetization is defined as a constant quantity for the bulk material. In the case of films, such as metallic wafers, this definition may no longer be legitimate. Since ferromagnetism arises from atomic interactions of a cooperative nature, it is anticipated that, as the number of atom layers in a film is reduced, three-dimensional effects will begin to disappear at some critical thickness and the behavior of the film will approach that of a paramagnetic material. Fortunately, as the critical thickness at which M_s is reduced is typically of the order of 30 \AA for most common ferromagnetic materials, the initial saturation magnetization of the cobalt films studied in this research (3200 \AA -thick) could be equated to the saturation magnetization of the bulk material (1400 emu/cm^3). This was supported by

calculating a theoretical saturation magnetization of 1369 emu/cm^3 for a 3200 \AA -thick *hcp* cobalt film grown by electron beam deposition. Finally, the detection coil geometries are usually described by assuming that the sample acts as pure dipole, which is true only for ellipsoidal samples or when the sample dimensions are very small compared to the dimensions of the detection coils. Therefore, corrections for sample size were applied to the calculated values of μ_s .

Assuming that the value of the saturation magnetization, M_s , is not affected by corrosion phenomena, the mass loss due to corrosion was calculated by:

$$\Delta m = \frac{\mu_{s,0} - \mu_{s,f}}{\mu_{s,0}} \cdot m_0 \quad (5)$$

where $m_0 = \frac{\mu_{s,0}}{M_{s,b}} \rho$ is the initial mass of cobalt, $\mu_{s,0}$ the saturation moment before exposure to the electrolyte, $\mu_{s,f}$ the saturation moment after a certain exposure time, $M_{s,b}$ the bulk cobalt saturation magnetization, and ρ the density of cobalt (8.832 g/cm^3). Corrosion rates were calculated by plotting the cumulative mass loss *versus* time, performing polynomial fitting, differentiating the fitting expressions over time, and normalizing to the exposed area.

Bare Samples

A typical potentiodynamic curve for uncoated cobalt on silicon wafer is shown in Figure 2. Both the cathodic and the anodic reactions are found to be under activation control. The

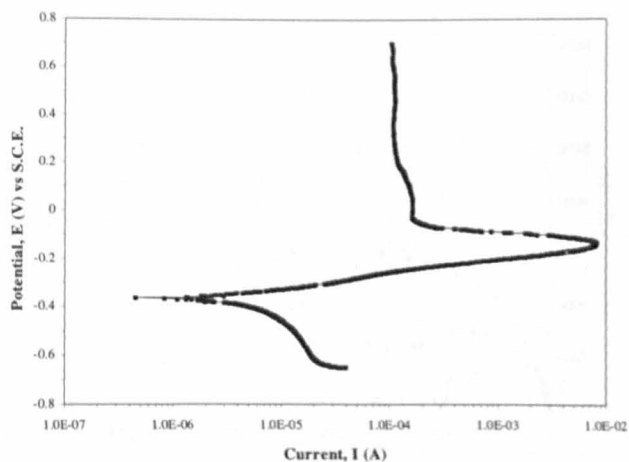
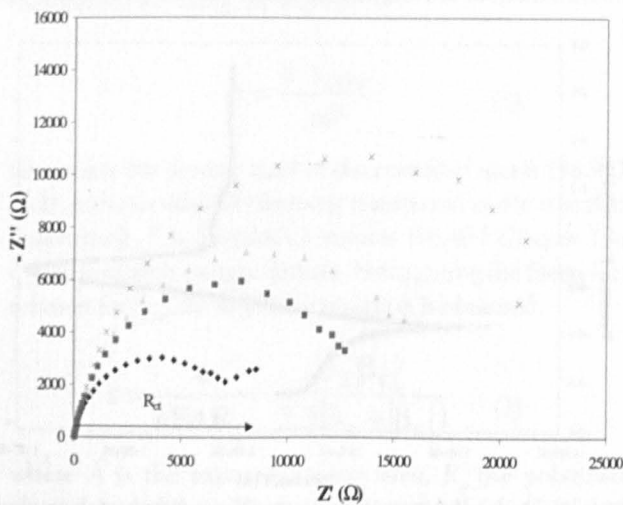
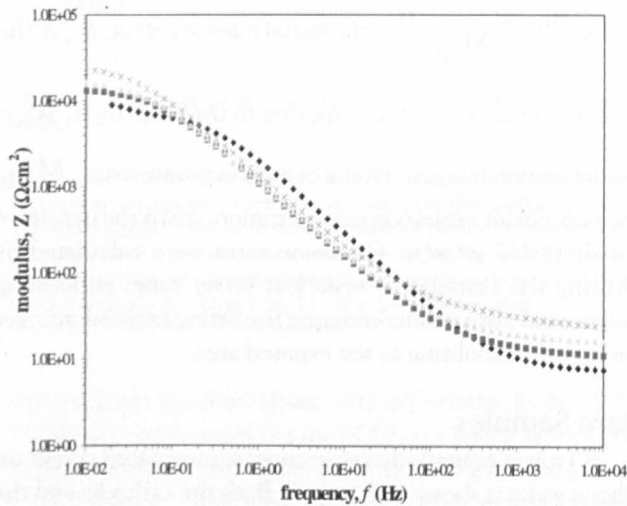
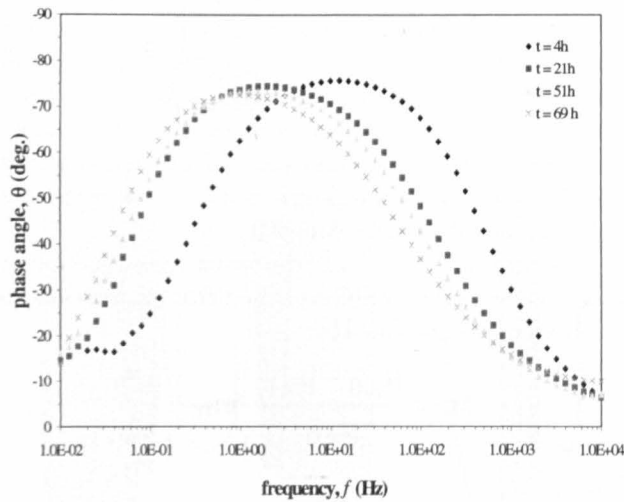


Figure 2: A typical potentiodynamic curve for uncoated cobalt on silicon wafer. Regions of activation polarization, concentration polarization and hydrogen evolution are marked along the cathodic curve by I, II and III, respectively.



cathodic polarization curve indicates oxygen evolution with mixed polarization, the combination of activation polarization and concentration polarization. The initiation of hydrogen evolution is also evident at lower potentials.

The average corrosion potential of cobalt on silicon wafer was found to be approximately -390 mV vs. SCE. This value lies between the standard potentials of cobalt and oxygen (-518 mV and -159 mV, respectively, vs. SCE). The anodic (β_a) and cathodic (β_c) Tafel constants were obtained by linear regression. Because of the presence of mixed polarization, the cathodic Tafel constant was estimated starting from a potential 30 mV below the corrosion potential (rather than 50 mV below this potential). The anodic Tafel constant was estimated starting from a potential 50 mV higher than the corrosion potential. A series of potentiodynamic measurements thus yielded: $\beta_a = 81$ mV and $|\beta_c| = 367$ mV.

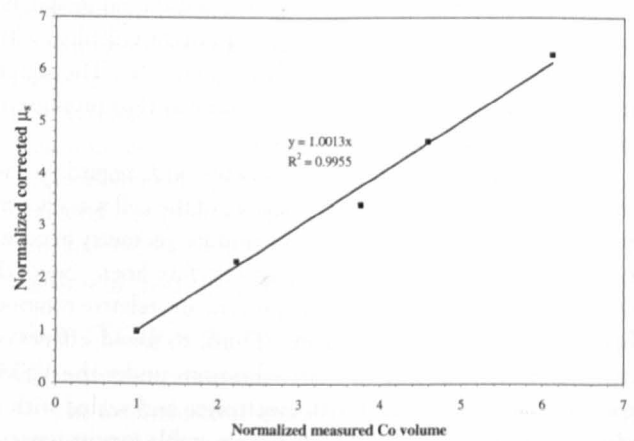


Figure 4: Correlation between the normalized saturation magnetic moment after sample size corrections and the volume of cobalt estimated from dimension measurements. Width of all samples: 0.65 cm. The line's equation and the correlation factor are included.

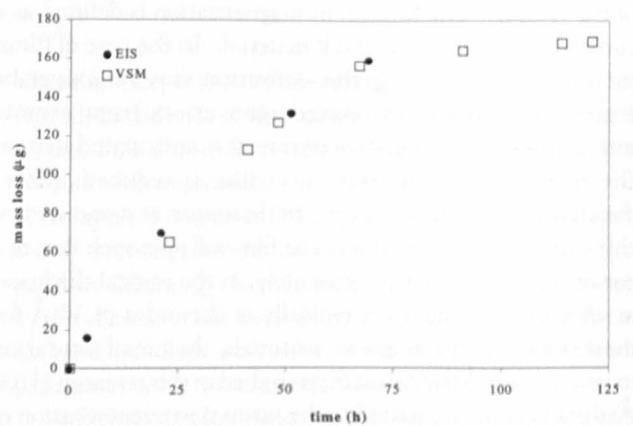


Figure 3: EIS Bode and Nyquist plots for bare cobalt after: a) 4, b) 21, c) 51, and d) 69 hours of immersion.

Figure 5: Cumulative mass loss of bare cobalt, as obtained from EIS and VSM measurements.

It should be noted that the literature reports that the absolute values of the Tafel constants usually range from 30 to 200 mV. Thus, the value of β_c reported above might seem too high. However other workers also suggest that experimental β_a values range from 60 mV to about 120 mV, while b_c values range from 60 mV to infinity, the latter corresponding to diffusion control by a dissolved oxidizer.

Figure 3 presents the EIS Bode and Nyquist plots for the uncoated cobalt metal with increasing times of exposure to the electrolyte. The charge-transfer resistance, or polarization resistance, was measured as the difference between the two plateaus in the modulus plots. Similar values were obtained by measuring the real axis chord of the depressed semicircle in the Nyquist plot. Sweeps performed at times longer than 69 h of immersion yielded spectra that could not be deconvolved for analysis. Such behavior may result from the

significantly reduced volume of cobalt and the exposure of the silicon wafer. The exposure of the silicon substrate after long immersion periods was observed, for example, in polymer-coated samples different from the ones described within this paper, by means of atomic absorption spectroscopy (AAS) and X-ray mapping using environmental scanning electron microscope (ESEM). Finally, large greenish and brownish spots were visually observed on the surface of the bare samples after only a few hours, suggesting the formation of $\text{Co}(\text{OH})_2$.

The effect of sample volume on the magnetometer output was examined experimentally. Normalizing both the volume of cobalt in each sample (assuming a uniform thickness of 3200 Å and neglecting errors in dimension measurements) and the corrected values of magnetic moment to a control sample, Figure 4 is drawn. Excellent correlation between the volume of cobalt and the moment values measured by the VSM is

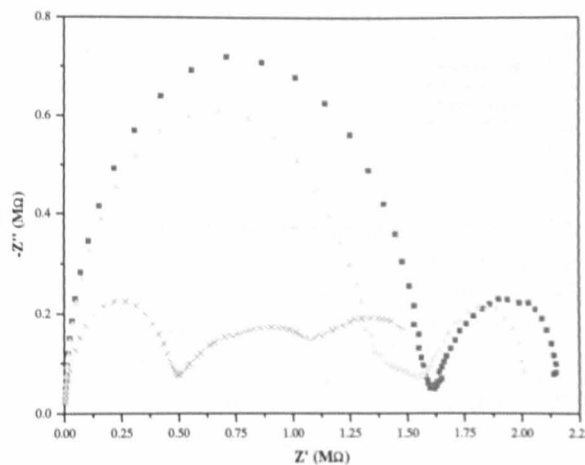
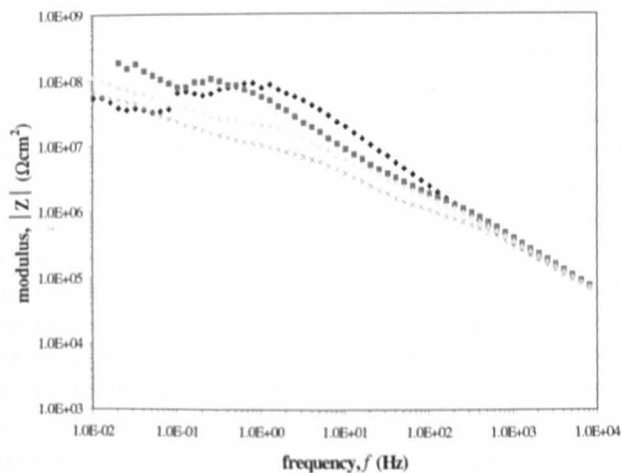
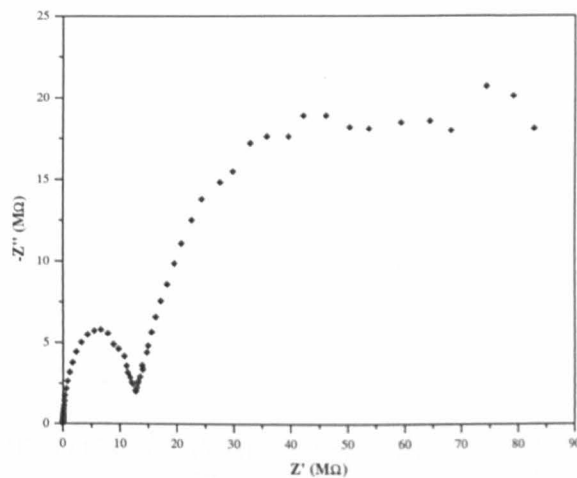
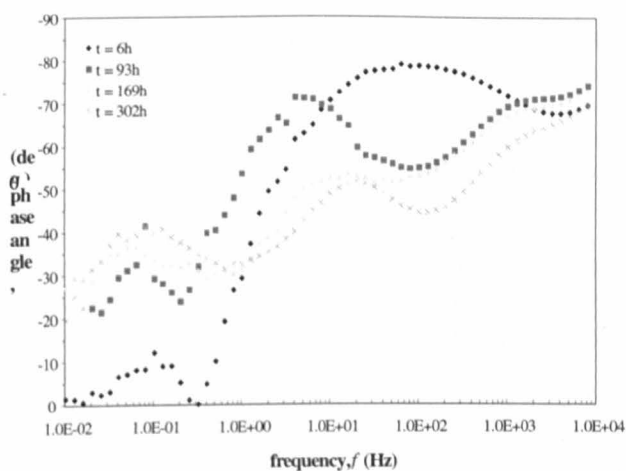


Figure 6: EIS Bode and Nyquist plots for acrylic-coated cobalt (sample #1) after: a) 6, b) 93, c) 169, and d) 302 hours of immersion. Only plots b and c may be used for the determination of R_{ct} , as evident from the Nyquist spectra.

evident from a line with a slope of approximately 1. This result is in accordance with the excellent correlation between VSM and gravimetric measurements reported by the authors elsewhere. Thus, the VSM is proven to be applicable for mass loss measurements.

Excellent correlation between the cumulative mass loss values measured by EIS and VSM is also evident for uncoated silicon/cobalt wafers (Figure 5). These results support the validity of determining R_{ct} (or R_p) directly from the Bode/Nyquist plot under such conditions. It is also evident from Figure 5 that the corrosion rate (proportional to the slope of the curve) decreases with time. This behavior is typical for corrosion of bare metals. Finally, the curve exhibits asymptotic behavior, which indicates that all of the initial mass of cobalt in the exposed area ($\sim 170 \mu\text{g}$) was consumed by corrosion after immersion for about 120 h.

Coated Samples

In the case of polymer-coated samples, EIS analysis could

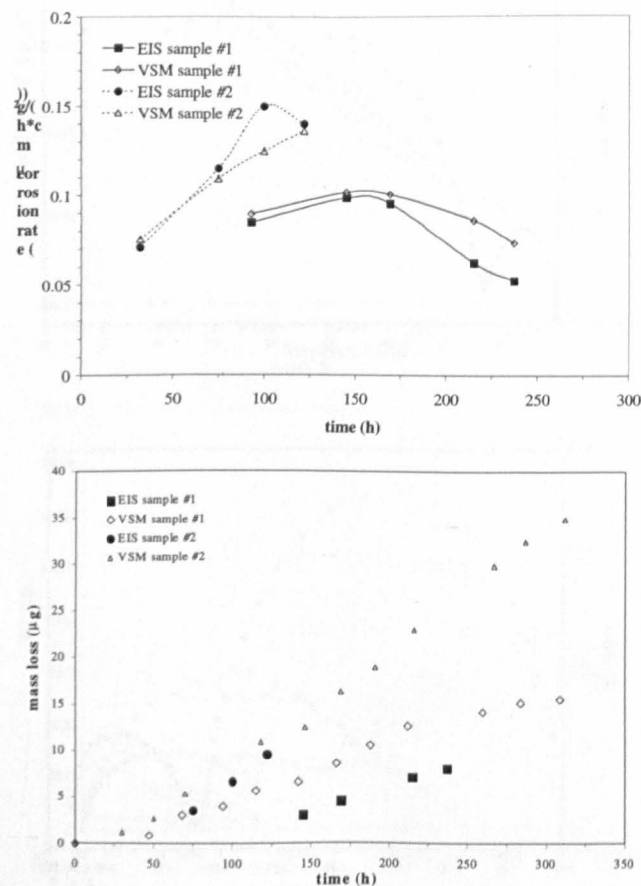


Figure 7: Underfilm corrosion rates (a) and cumulative mass loss (b) of polymer-coated cobalt samples, as obtained from EIS and VSM measurements.

only be made after some immersion time, when the cobalt beneath the polymer was clearly exposed. This was reflected by the appearance of a second semicircle at low frequencies

(Nyquist plot). EIS analysis was also not possible after long immersion times, likely due to masking effects of diffusion through corrosion products, which had formed at the bottom of defects in the coating, and/or exposure of the silicon substrate (as previously discussed). Selected Bode and Nyquist plots for the coated samples are shown in Figure 6.

Figure 7(a) reveals the underfilm corrosion rates of polymer-coated cobalt samples, as obtained by both EIS and VSM measurements. The corrosion rates increase with exposure time, reach peak values and subsequently decrease, as typical for coated samples. Moreover, lower mass losses were observed (Figure 7(b)) for the coated samples in comparison with the uncoated samples (Figure 5), as anticipated. Visual and microscopic observations indicated that corrosion initiated at defects, and usually progressed in a branch-like fashion. The slightly different corrosion rates observed for the two coated samples likely resulted from differences in the distribution of defects in the acrylic coating. Good agreement between the corrosion rate values obtained from EIS and VSM measurements is apparent in Figure 7(a). Discrepancies in data between the two techniques may result from changes in the Tafel parameters with time and inaccurate determination of R_{ct} from the Bode and Nyquist plot. The good agreement between EIS and VSM results supports, for the first time, the validity of using R_{ct} and the Stern-Geary relation (equation 2) for underfilm corrosion rate evaluation. However, as shown here, such an evaluation can be made on the basis of EIS only well after corrosion initiates, and when diffusion (or other) processes do not mask the appearance of the substrate in the EIS spectra.

Outlook

As shown in this article, there are currently several difficulties in interpreting the EIS spectra. Experimental approaches that can overcome masking effects are currently under investigation. In addition, efforts to deconvolve the EIS spectra and to better define equivalent circuits with the aid of VSM results are in progress. For example, one may use the VSM to enhance the interpretation of EIS data through the following procedure: (1) measure the mass loss by means of a VSM; (2) use this mass loss value to determine R_p (equation 2); (3) examine the EIS spectra carefully and isolate the feature that most likely corresponds to the pre-determined R_p .

Measurements of the magnetic moment have some additional potential applications with regard to corrosion of either ferromagnetic or non-ferromagnetic materials. Firstly,

because it is easy to monitor the underfilm corrosion of cobalt using a magnetometer, this material could be used as a corrosion tracer (e.g., in electronic device packaging). Secondly, magnetic measurements may be applied to other ferromagnetic materials such as iron. Most iron oxides are ferromagnetic. However, at low pH they are unstable, thus possibly allowing monitoring the corrosion of iron in acidic environments. Thirdly, it may be possible to apply magnetic moment measurements for corrosion monitoring of paramagnetic as well as diamagnetic metals. The magnetic moment, $m(H)$, of a paramagnetic material is proportional to the applied magnetic field:

$$\mu(H) \equiv V \cdot M(H) = V \cdot \chi \cdot H \quad (6)$$

where $M(H)$ is the magnetization, V the volume of the material, χ the magnetic susceptibility, and H the magnetic field. The only dependence of the magnetic susceptibility of a paramagnetic material is on temperature, although it is nearly constant within a range of hundreds of degrees [34]. Using a magnetometer, one can measure the slope of this line, $\alpha = V \cdot \chi$, after different exposure periods. If all measurements are carried out approximately at the same temperature, one gets:

$$\frac{\alpha_i}{\alpha_o} \cong \frac{V_i}{V_o} \quad (7)$$

where i and o denote exposure times $t = i$ and $t = 0$, respectively. This equation may be rearranged as:

$$\frac{\Delta\alpha}{\alpha_o} \cong \frac{\Delta V}{V_o} = \frac{\Delta m}{m_o} \quad (8)$$

Thus, the VSM may be used to monitor the corrosion of polymer-coated paramagnetic metals if the signals of both coating and corrosion/oxidation products are negligible compared to that of the bulk metal. This technique may be applicable to metals such as aluminum, magnesium and titanium. Similarly, the technique may be applied to diamagnetic metals such as copper, cadmium and zinc. However, any application of this kind requires enough data on the magnetic properties of both the corrosion/oxidation products and the polymer coating (if it exists). Finally, advances in instrumentation for magnetic moment measurements may allow *in situ* and in real time monitoring of the underfilm corrosion in larger parts in the field.

Conclusions

Based on *in situ* measurements of the corrosion rate for

both bare and acrylic-coated cobalt samples by means of EIS and a VSM, the following conclusions are drawn:

1. Measurements of the saturation magnetic moment allow accurate *in situ* monitoring of corrosion rates of bare and polymer-coated cobalt.
2. Magnetic measurements may be used to improve the interpretation of EIS data, especially with respect to underfilm corrosion.
3. When the charge-transfer resistance can be determined unambiguously from EIS spectra, underfilm corrosion rates can be measured.
4. The use of magnetic measurements for monitoring underfilm corrosion may be extended to other materials, including paramagnetic and diamagnetic ones.

Acknowledgements: This work is partially supported by the National Science Foundation (NSF) through grant number DMR-9708148. This work has been carried out on a collaborative basis by N. Eliaz¹, D.B. Mitton¹, N.J. Cantini¹, G. Leisk¹, S.L. Wallace¹, F. Bellucci², G.E. Thompson³ and R.M. Latanision¹. Interest in taking this work further through collaboration is welcomed and in the first instance contact should be made with N. Eliaz of the H.H. Uhlig Corrosion Laboratory, Massachusetts Institute of Technology, Cambridge, MA 02139, USA. Tel: (+1) (617) 253-5260, Fax: (+1) (617) 253-8745, E-mail: neliaz@mit.edu

Controlled Hydrothermal Production Of Hydroxylapatite From Marine Skeletons

Hydroxylapatite is a biocompatible ceramic material which is widely used within the biomaterials industry. The synthesis of hydroxylapatite from a Mexican native marine skeleton (Mellite Eduardobarrosoi sp. Nov.), based on a thermal treatment at 800°C, for 2 hours may provide a valuable and cost effective source of this commodity. Calcium oxide (CaO) is produced in a first stage, this compound as well as monetite (CaHPO₄) is precursor of hydroxylapatite. The reaction between these two precursors was carried out under hydrothermal conditions at 1.4 MPa for